Suction optimization on thick airfoil to trap vortices

Raffaele S. Donelli[1], Pierluigi Iannelli[1], Emiliano Iuliano[1], Donato De Rosa [1]
[1] *Physics and Fluids Unit, Centro Italiano Ricerche Aerospaziali (CIRA), Via Maiorise, snc, 81043 Capua (CE), Italy*
E-mail: r.donelli@cira.it, p.iannelli.@cira.it, e.iuliano@cira.it, d.derosa@cira.it

Keywords: Trapped vortex, pressure drag reduction, flow control.

SUMMARY. A trapped vortex device is a cavity to trap flow vortices to reduce pressure drag levels past bluff bodies and/or thick wing airfoils. Preliminary studies showed the need to apply a constant mass flow suction inside the cavity to stabilize the vortex. The aim of this work is to find the best location and the minimum suction distribution to be applied in the trapped vortex mounted on a NACA0024 airfoil to be tested in the 3 diameter wind tunnel section of the Politecnico of Turin in order to delay flow separation. This activity has been carried out in the framework of the European project VCELL2050.

1 INTRODUCTION

This work has been developed in the framework of the European program VCELL2050 (Vortex CELL 2050) whose main objective is to demonstrate that the proper design of cavity shapes to trap flow vortices can be effective to reduce pressure drag levels past bluff bodies and/or thick wing airfoil [1]. Preliminary basic studies were performed by using an airfoil mounted on the wall test section [2] of the CIRA CT-1 wind tunnel. It was demonstrated that trapping and stabilizing a vortex on the upper surface of the test bed by using a constant mass flow suction inside the cavity, allows to achieve fully attached flow past the cavity at high incidences. Unfortunately, in this experiment pressure drag and lift measurements were not available, given the experimental set-up. As a consequence, further experimental tests on an industrial wing model have been planned in the POLITO wind tunnel. The objective will be to show the benefits/detriments, in terms of the aerodynamics performances, coming from the use of this flow control technique by estimating drag and lift coefficient with respect to the energy needed for suction. The test case is the NACA 0024 thick airfoil equipped with a cavity on its upper aft surface whose shape and location has been optimized to allow for the vortex trapping. The optimization process has been carried out at a fixed pre-defined angle of attack where flow separation is expected on the clean airfoil. On the other hand, one of the lessons learned during experimental tests in CIRA facilities is that, at high incidences, it is not possible to stabilize the vortex inside the cavity without a suction system. As a consequence, it is necessary to estimate the mass flow suction rate and its location inside the cavity. A possible region to play suction in the cavity has been already individuated on the basis of the previous studies performed on the CIRA test bed. It is quite obvious that the success of this technique is connected to the energy needed to stabilize the vortex in the cavity. The main objective of this work is to perform a parametric study aimed at individuating, for a given pump suction power, the trends towards the minimimzation of airfoil pressure drag and cavity suction energy able to stabilize and reattach the flow. This will help to drive the POLITO experiments on the wing model.

2 POLITO wind tunnel esperiments

A test campaign on a 2-D NACA0024 airfoil equipped with a trapped vortex is planned in the VCell2050 project. The objective is to demonstrate the feasibility and the effectiveness of the trapped

vortex flow control technique to reduce pressure drag and to increase lift in high lift conditions. Lift and drag measurements will be performed on the clean airfoil, as well as, on the airfoil equipped with a trapped vortex cavity. Successively, the clean aifoil will be equipped with a classic suction system achieved by covering the cavity region with a porous wall. The aim is to have an idea of the advantages coming from the use of the trapping cavity with respect to the massive suction. Since the cavity is provided of a suction system to stabilize the vortex inside the cavity it is necessary to know what are the values of mass flow rates to be applied and where. The experimental tests will focus mainly on the 14° angle of incidence and 30 m/s wind tunnel speed, for which the cavity was designed. Then several angles of incidence will be investigated, as well as some wind tunnel speeds. The wind tunnel model will be vertically installed in the test section and two horizontal planes located at the extremities of the wind tunnel model will assure the two-dimensionality of the flow. The chord of the model is 500 mm and its spanwise lenght is 1200 mm. The numerical investigations, that will be presented in this paper, have been performed in wind tunnel flow conditions.

3 Geometries and suction slots locations

The well known NACA0024 airfoil was selected for testing the trapping vortex (TV) cavity concept, since it belongs to the class of thick airfoils whose flow separation control is the main aim of the VCELL project [3]. In the turbulent regime, the NACA0024 airfoil has a smooth stall separation which increases in size and moves upstream as the incidence increases. Flow separations over thick airfoils can be manipulated by the usage of suitable trapping cavities. In this work, two airfoil geometries have been numerically investigated and are shown in Figure 1:

- Clean NACA0024 airfoil (baseline)
- A modified NACA0024-TV airfoil having a trapping cavity on its upper surface

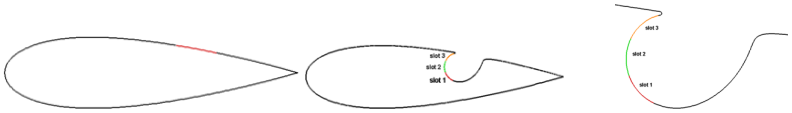

Figure 1: Baseline NACA0024 and NACA0024-TV airfoil - Detail of suction slots (colored curves).

NACA0024 Clean airfoil	NACA0024-S Clean airfoil with distributed suction
NACA0024-TV	TV airfoil - no suction
NACA0024-TV-S1	TV airfoil - suction on slot 1 only
NACA0024-TV-S2	TV airfoil - suction on slot 2 only
NACA0024-TV-S3	TV airfoil - suction on slot 3 only
NACA0024-TV-SALL	TV airfoil - suction on all slots

Table 1: Summary of airfoil/suction location configurations considered.

The first is the geometry of the clean airfoil without and with a distributed suction system located on the rear part of the upper surface of the airfoil and indicated by the red line. The second geometry is the airfoil equipped with the trapping cavity. The shape of the cavity has been designed within the VCELL project [1]. In Figure 1 both locations and typical size of the suction slots have been reported for both configurations. In particular, for the TV-airfoil, three contiguous suction regions in the cavity have been manufactured, having approximately the same area. In Table 1 a summary of all the airfoil and suction configurations is reported together with the relative nomenclature. The

extension of the distributed suction area is comparable to the overall suction area of the TV case, in order to have meaningful comparisons with both clean case and TV airfoil.

4 COMPUTATIONAL GRIDS

Computational grids have been generated for both the baseline and TV airfoil configurations. In particular, the computational domain considered includes the top/bottom wind tunnel walls, in order to account for their influence on aerodynamic performances. All the grids described in the following were designed for usage of wall-resolved turbulence modeling, i.e. the first grid cell center was placed at a distance from the wall corresponding to a value of $y^+ = 1$.

4.1 *Grid around NACA0024 Airfoil in the Wind Tunnel*

A hybrid grid made up of about 32.000 elements has been generated around the baseline configuration. The airfoil periphery was discretized by means of 460 elements stretched in both the leading edge and trailing edge area. By starting from this curve discretization, 30 layers of quadrilateral elements have been grown around the airfoil, in the normal to the wall direction, in order to properly capture the viscous boundary layer. The remaining area of the computational domain was covered by means of triangles. No stretching was placed in the direction normal to the wind tunnel walls, since such walls were treated as inviscid in the solution phase. According to the experimental procedure, where the effect of the freestream angle of attack is reproduced by means of an airfoil rotation, also in the computational case several airfoil rotations have been considered and for each of them a grid has been generated. Figure 2 shows the mesh generated for the 14° incidence case.

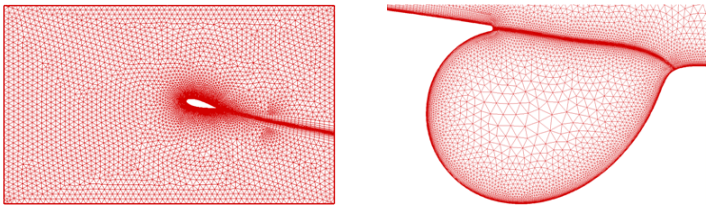

Figure 2: Hybrid grid around the NACA 0024 airfoil (14 degs airfoil rotation) - Cavity grid detail

4.2 *Grid around NACA0024-TV Airfoil in the Wind Tunnel*

A similar grid generation strategy was used to build the grid around the airfoil with the cavity. In this case a structured grid (30 layers of quadrilateral elements) was placed in the viscous regions such as the boundary layer region around the airfoil, along the cavity periphery and also in the shear layer running through the cavity opening (i.e., the region between the cusp point and the opposite knee). All the rest of the domain was covered by triangles, ending up with an overall grid size of about 51.000 elements. The airfoil periphery, excluding the cavity part, was discretized by means of 540 elements stretched close to the trailing edge, close to the cusp point and at the trailing edge. The cavity periphery was discretized by means of 360 elements, leading to the very refined grid shown in Figure 2. Larger mesh sizes are used in the cavity center since inviscid flow is expected there. Each angle of attack was achieved by proper rotation of the airfoil and subsequent grid generation.

5 Flow Solvers and Boundary Conditions

The $FLUENT^{\mathbf{TM}}$ commercial code was used to perform the numerical simulations, since it was already validated within the VCELL project [1, 2]. As a matter of fact, at this stage of the

project a great knowledge has been gained about the usage of such a code for simulating trapping cavity flows and a lot of information regarding both numerical and modelling settings have been acquired from previous validation activities. The $FLUENT^{TM}$ code solves the Reynolds Averaged Navier-Stokes (RANS) flow equations on hybrid grids by means of the Finite Volume method.

5.1 *Employed Numerical Algorithms*

A second order UPWIND scheme was utilized for the spatial reconstruction of convective fluxes whereas a cell-centred scheme is used in FLUENT to treat diffusive fluxes. Moreover, due to the incompressible formulation utilized, the continuity is enforced by means of a Poisson equation for pressure. The so-called "pressure-based coupled algorithm" was used to solve the steady-state equations, where both the momentum and pressure Poisson equations are solved together. The coupled scheme obtains a robust and a very efficient single phase implementation for steady-state flows, with superior performance compared to other solution schemes. The full implicit coupling is achieved through an implicit discretization of pressure gradient terms in the momentum equations, and an implicit discretization of the face mass flux, including the Rhie-Chow pressure dissipation terms [4]. The pressure-staggering (PRESTO!) approach was used in enforcing the discrete continuity balance and, based on past experience, the k-ω SST turbulence model was selected to account for turbulence effects, since it demonstrated to be accurate in reproducing flows inside trapping cavities.

5.2 *Boundary conditions*

The following boundary conditions have been used to carry out the flow computations:

- **WT test section entrance:** on the inlet computational domain, a velocity inlet type boundary condition was used. The velocity vector component in the x-direction was set to 30 m/s, the turbulence viscosity ratio $\frac{\mu_T}{\mu_L}$ was set to 1.5 and the turbulence intensity I_t was set to 0.1
- **WT test section exit:** on the outlet of the computational domain a pressure outlet type boundary condition was used. It requires the specification of the static pressure (ambient conditions) only, whereas the solver extrapolates all other quantities from the domain.
- **Suction on upper surface airfoil and in the cavity:** since the flow re-attachment is attained by means of suction a velocity inlet type boundary condition was used to achieve the required suction flow rate. A negative normal velocity component was set in order to get the desired mass flux exiting the computational domain.
- **WT walls:** the computational effort was reduced by generating an inviscid grid type close to the wind tunnel walls since there was no interest in accurately reproduce the wind tunnel wall boundary layer. The shear stress on the cell faces located on such boundaries was set to zero.
- **Airfoil walls:** classical no-slip boundary conditions were used there.

6 Results

In the following the numerical results will be illustrated and compared. All the computations were run for a wind tunnel speed of 30 m/s, which correspond to a Reynolds number of one million, based on the airfoil chord and standard atmosphere conditions at sea level.

6.1 *CFD Analysis of NACA 0024 Airfoil*

A first set of computations was run for the baseline airfoil. The aerodynamic performances obtained from such calculations were used next to quantify the potential benefits achievable by the

trapping cavity concept. On the left of Figure 3, it is shown the lift curve obtained from the current in-tunnel flow computations. Pressure distributions over the airfoil for several incidences are shown in the other two diagrams. As it can be observed, at both $14°$ and $18°$ of incidence the wide plateau region in the rear of the airfoil upper surface indicates severe separation. This is confirmed by Figure 4, where the skin friction coefficient over the airfoil is reported. At $5°$ of rotation there is a small separation starting at about 90% of the airfoil chord (black circles). The separation point moves at about 75% at $10°$ and than to 56% and to 30% of the chord for $14°$ and $18°$ of incidence, respectively.

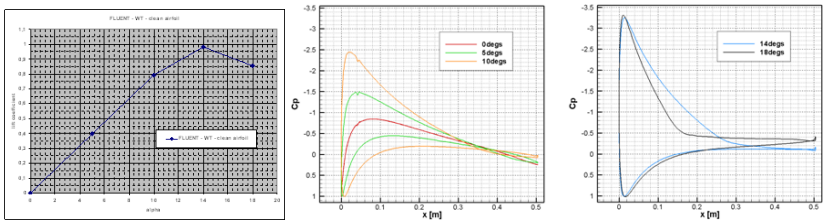

Figure 3: Lift curve and pressure distributions on the NACA 0024 clean airfoil in WT conditions.

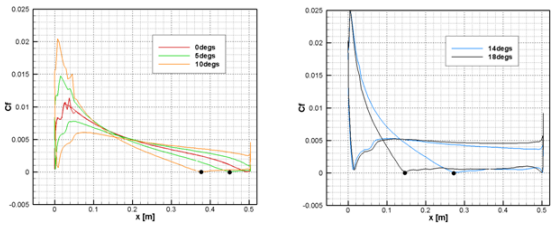

Figure 4: Skin friction coefficient on the NACA 0024 clean airfoil in WT conditions.

α	C_l	C_d
0	0,001	0,0148
5	0,398	0,0165
10	0,793	0,0245
14	0,981	0,0437
18	0,855	0,1005

Table 2: Aerodynamic coefficients for NACA0024 airfoil at in-tunnel conditions

Finally, Table 2 shows values of lift/drag coefficients obtained from the current computations.

6.2 *CFD Analysis of NACA0024-TV Airfoil*

A summary of the results obtained for the NACA0024-TV airfoil by considering different combinations of suction locations/mass flow rates for each incidence analysed are reported. In order to simplify the discussion of the results, the nomenclature indicated in Table 1 will be used to specify suction locations inside the cavity.

6.2.1 *NACA0024-TV at $\alpha = 0°$ (no-suction)*

A first computation was run for the NACA0024-TV airfoil at $\alpha = 0°$ angle of attack. In Figure 5 the streamlines both around the airfoil and inside the cavity are reported, showing attached flow on

the airfoil surface. A vortex is trapped in the cavity without requiring any kind of suction. Both the turbulent viscosity ratio $\frac{\mu_T}{\mu_L}$ and velocity magnitude contours, showed in figure 5, confirm this flow behaviour, already observed for past cavity shapes investigated within the VCELL project [2].

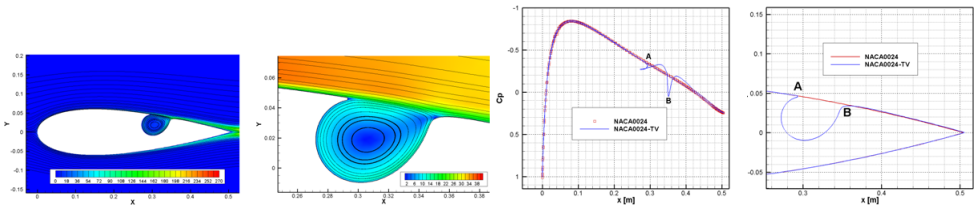

Figure 5: NACA0024-TV airfoil. Streamlines and turbulence viscosity ratio $\frac{\mu_T}{\mu_L}$ contours at 0° - Details of the cavity region - Comparisons of surface pressure coefficient and geometries between clean NACA0024 and NACA0024-TV airfoil.

In Table 3 a comparison of the force coefficients is reported between the TV airfoil and its baseline counterpart, showing that the presence of the cavity produces only a very small increase in lift and a very small increment in drag, which is mainly due to a different pressure distribution on the airfoil. As a matter of fact, from the post-processing of the CFD solution it came out that the friction drag coefficient of the TV airfoil was smaller (86 drag counts) than the clean airfoil (91 counts). The reason for such reduction is that the TV-airfoil flowfield has a reversed flow region (i.e. the inner cavity flow) where negative friction drag is locally generated. Therefore, the overall increment of drag is due to an increment of the pressure drag which is likely due to the presence of an additional stagnation point in the airfoil flowfield.

Airfoil	α	C_l	C_d
NACA0024	0	0,001	0,0148
NACA0024 - TV	0	0,013	0,0156

Table 3: Aerodynamic coefficients of NACA0024 and NACA0024-TV airfoils.

On the right of Figure 5 it is reported a comparison of pressure distributions for the two airfoils analyzed, showing that the presence of the cavity only slightly alters the symmetric pressure distribution of the clean airfoil, giving rise to small changes in the aerodynamic forces observed in the above table. It is worth noting that the pressure distribution is almost unaltered by the presence of the cavity in the regions of the lower airfoil surface and on the upper surface, upstream of the cavity (see point A). The point B represents the downstream stagnation point of the cavity flow, and it can be observed from the pressure that by moving from point B to the left, the flow inside the cavity undergoes first a significant acceleration, next it starts to very gradually decelerate and finally it re-accelerates up to the cusp point A. The above gradual deceleration inside the cavity demonstrates the effectiveness of the design activity, in which one of the requirements driving the cavity shape design was the minimization of the adverse pressure gradient in the cavity, in order to avoid the presence of secondary separations. Moreover, moving from point B to the right there is a local region of expansion and favourable pressure gradient, followed by the typical regular recompression region.

6.3 *NACA0024-TV at 14 degrees incidence with and without suction*

A new set of computations was run by considering the NACA0024-TV airfoil set at several incidences. The first flow configuration chosen to test the TV concept corresponds to a rotation of

14 degrees. As already mentioned, at such flow condition there is a large separation on the baseline airfoil, therefore it represents a meaningful flow condition to challenge the trapping cavity concept. In Figure 6 it is shown that at such a high incidence the cavity alone is not able to capture a vortex and therefore to suppress/delay the separation.

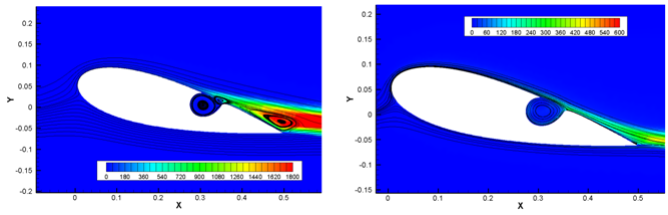

Figure 6: NACA0024-TV airfoil. Streamlines and turbulence viscosity ratio $\frac{\mu_T}{\mu_L}$ contours at 14° - without suction (left) and with distributed suction on all slots (right) (MFR=0.08Kg/ms).

It was decided to test the TV concept effectiveness playing suction in the cavity periphery, according to the locations shown in Figure 1. It was decided to play a uniformly distributed suction by using all the available slots at the same time (NACA0024-TV-SALL configuration) and it was numerically found that with a suction MFR value of 0.08 (Kg /ms) the vortex is trapped in the cavity, the downstream flow is reattached and the separation point is shifted to 91% of the chord, as shown in Figure 6. However, as it was experienced in CFD calculations, increasing/decreasing the suction MFRs produces slightly changes in the trapped vortex characteristics and moves the separation further downstream/upstream.

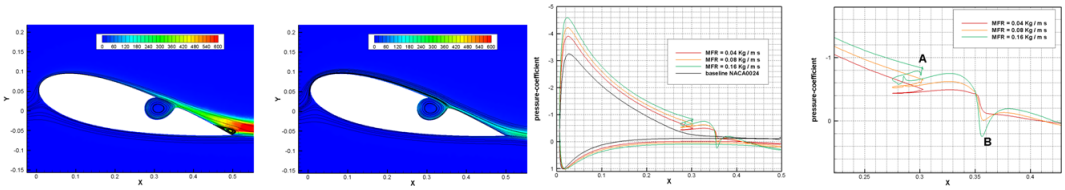

Figure 7: NACA0024-TV airfoil. Streamlines and turbulence viscosity ratio $\frac{\mu_T}{\mu_L}$ contours at 14° - Distributed suction on all slots. MFR = 0.04 Kg /m s (1^{st} picture) and MFR = 0.16 Kg /m s (2^{nd} picture) - Pressure coefficient distribution for several MFRs. Overall Cp distribution (3^{rd} picture) and zoom in the cavity region (4^{th} picture).

As an example of such an effect, in Figure 7 it is shown the difference in the flowfield both at higher and lower MFRs. On the right of the same figure, the pressure coefficient on the airfoil surface is plotted for several MFR values discussed above and compared with the baseline airfoil pressure distribution. As it can be observed, an increased suction in the cavity produces a faster vortex with a consequent "suction effect" upstream, which increases the overall airfoil's circulation. The surface pressure coefficient in the cavity region highlights the quite different flow behavior obtained depending on the suction level. In fact, for MFR=0.04 Kg/ms, only a small acceleration inside the cavity is visible, whereas the typical downstream expansion is absent. On the other hand, for higher MFRs the expansions occurring after the cavity stagnation point (both inside the cavity and in the airfoil rear part) tend to be more and more amplified as the MFR increases. The different cavity flow behaviour observed for the three MFRs considered has a non trivial impact on the flow behaviour downstream the cavity, therefore influencing also the separation point location. In fact, as shown in

Figure 8, in the MFR=0.04 case after the stagnation region (i.e., moving in the right direction) there is no flow acceleration, the inviscid flow is quite slow and the boundary layer is yet quite thick and not very full. On the other hand, from the same figure, it can be observed that by increasing the MFR the stagnation regions moves slightly upstream, the inviscid flow acceleration increases more and more, the boundary layer gets both thinner and fuller and it can therefore resist for a longer distance to the adverse pressure gradient, leading to a downstream shifting of the separation point.

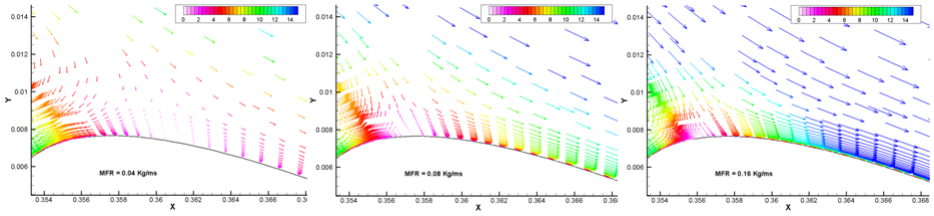

Figure 8: NACA0024-TV-SALL airfoil. Velocity vectors (m/s) in the cavity at 14 degs MFR = 0.04 Kg /m s (left), MFR = 0.08 Kg /m s (center) and MFR = 0.16 Kg /m s (right).

Figure 9 shows the evolution of the downstream separation point as a function of the suction MFR, confirming the considerations made above. The results shown herein have suggested studying the TV concept in the framework of a parametric approach, by changing alternatively incidence, suction location and suction MFR.

6.4 *Parametric study on the effects of slot location/mass flow rate*

An analysis of the lift and drag coefficients as a function of both suction location and MFR has been performed. It must be remarked that in the lift/drag forces bookkeeping, the contributions associated to the suction jets have been also accounted for, by performing proper pressure and momentum integration over the involved suction areas. In Figure 9 the lift/drag coefficients are plotted as a function of the MFR, for different suction locations at 14° of incidence. As it can be observed, for fixed MFR the lift is almost unaffected by the suction location, whereas it increases as the amount of suction increases. The drag coefficient is affected by the suction location and the slot 3 results to be the most effective place to play suction, since it seems to minimize the drag. From post-

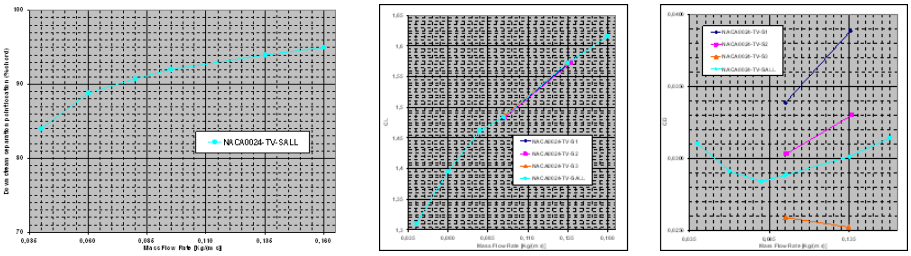

Figure 9: NACA0024-TV-SALL airfoil @ 14 degs. Separation point locations versus suction MFR - Lift and Drag coefficients as function of both suction MFR and slot location.

processing of the CFD data, it emerged that the (reaction forces) contributions associated to both pressure and momentum integration over the suction slots were almost negligible for all the flow conditions/slots-locations considered, except the drag component associated to pressure integration over the slot(s). However, for the NACA0024-TV-S3 configuration the normal vector associated to

the slot surface is mostly oriented in the vertical direction and has only a small component in the horizontal direction, therefore providing the smallest contribution to the drag with respect to the other suction configuration considered. Moreover, the CFD post-processing also suggested that the reaction drag associated to the slot always grows as the MFR increases, whatever is the slot configurations considered. The rule of the slot location is not a trivial issue in designing a trapping cavity system, since the differences in drag can be as high as about 150 counts for fixed MFR, as it can be appreciated from Figure 9. This can strongly affetcs the aerodynamic efficiency that is an important parameter to account for in high-lift conditions. As a matter of fact, the aerodynamic efficiency reported in Figure 10 results to be maximized and has a growing behaviour for a large range of MFRs when using the slot 3, whereas it has less favourable behaviour when using the S1 or S2 configurations. Also in this case it must be remarked that differences as high as 20 can be achieved on the aerodynamic efficiency, depending on the suction slot location/MFR considered.

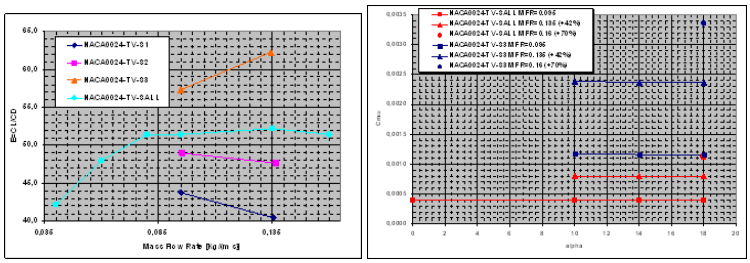

Figure 10: Aerodynamic efficiency as a function of both cavity suction MFR and slot location @ 14 degrees - Momentum coefficient C_μ vs. α for different levels of suction MFRs and slot locations.

The momentum coefficient $\int \rho V \mathbf{V} \cdot d\mathbf{S} / \left(1/2 \rho_\infty V^2 c\right)$ has been also calculated by numerical integration over the slot area from several CFD solutions available, in order to compare the current flow control concept with other concepts available in literature. As it can be observed from Figure 10, for fixed MFR the momentum coefficient changes by a factor 3 between the S3 configuration and the SALL configuration. This occurs since the S3 suction area is one third of the SALL suction area, and therefore the suction velocity must grow by a factor 3 to guarantee the same MFR. From this point of view, it must be observed that the SALL suction configuration provides slightly lower levels in terms of aerodynamic performance over the S3 configuration, but it could be much more convenient in terms of energy or power needed to realize the control.

6.5 *CFD Analysis of NACA0024 Airfoil with distributed suction (NACA0024-S)*

CFD computations have been carried on the baseline NACA0024 airfoil with added a distributed suction slot on its upper surface, located approximately in the same region of the trapping cavity opening. In order to have interesting comparisons, the NACA0024-S configuration will be compared with the NACA0024-TV-SALL performance, since they are characterized by the same suction area. The reaction forces associated to the suction jet have been accounted for in the CFD data post-processing. From this point of view, the slot location of the NACA0024-S is much more advantageous, since it provides a small additional drag and small, but positive, contribution to the lift (about 0.05). Figure 11 shows the comparison of both overall lift and drag coefficient as a function of the suction MFR for the two configurations considered. It must be remarked that one of the most important parameter in evaluating the performance of a flow control system is the MFR (and momentum coefficient) since it will be proportional to the power needed for the control. As observable

from the figure, the lift provided by the distributed suction is always lower than that obtained with the cavity+suction system, at the same MFR. Such a difference increases for low values of the MFR (i.e., when energy expenditure is low). Similarly, the drag of the distributed suction system is much higher at lower MFR when compared with the cavity+suction system. Accordingly, the aerodynamic efficiency results to be lower (about 20%) in the distributed suction case, at low MFRs, as shown on the right of Figure 11. These results demonstrate that the distributed suction concept is much less effective in suppressing the flow separation, since its drag curve minimum appears to be shifted much in the right side of the drag vs. MFR plot if compared to the cavity+suction concept. In other words, the distributed suction concept is able to suppress the flow separation and achieve even lower drag levels with respect to the cavity+suction system, but at the cost of much higher energy expenditure.

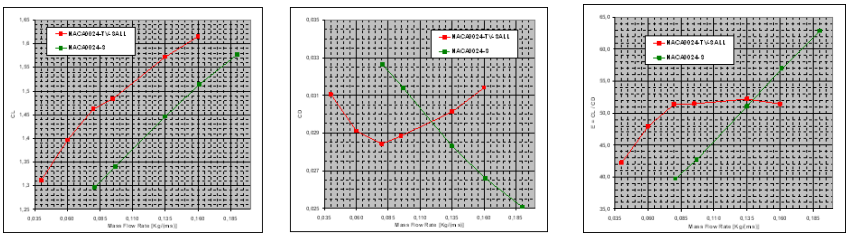

Figure 11: Lift and drag coefficients vs. MFR @14 degrees - Aerodynamic efficiency vs. MFR, for different flow control concepts tested - for different flow control concepts tested.

7 CONCLUSIONS

A CFD parameric study has been performed to analyze the flow characteristics of a cavity-equipped airfoil with vortex trapping and suction playing. Different values of the suction mass flow rate and of the suction slot locations have been considered. A comparison between the airfoil shape with no cavity + distributed suction and with trapped vortex cavity + suction has been carried out. The trapped vortex cavity resulted to be more effective with respect to the distributed suction either in terms of lift/drag coefficient either in terms of aerodynamics efficiency/required energy for the control. On the other hand, the cavity with distributed suction (SALL) was found to be the best compromise in terms of aerodynamic performances and energy or power needed to realize the control when compared to the S3 configuration. It has to be stressed that some margins of improvement in the suction location can be still foreseen: this could be numerically achieved through a real optimization process aiming at searching the optimal suction locations and mass flow rates which allows for the minimum value of the energy due to the suction system under fully attached flow/low pressure drag constraint.

References

[1] Donelli, R.S., Iannelli, P., Chernyshenko, S., Iollo, A., Zanetti, L.*Flow models for a vortex cell*, AIAA Jourbal, Vol. 47, No.2, February 2009, DOI: 10.2514/1.37662

[2] Donelli, R.S., De Gregorio, F., Iannelli, P., *Flow Separation Control By Trapped Vortex*, Submitted to the 48th AIAA Aerospace Sciences Meeting, Orlando (2010).

[3] **VCELL2050 - Vortex CELL scenario 2050** European project - Description of Work (DoW) (2005)

[4] FLUENT 6.1, Users Guide, February 2003